Electron. Mater. Lett., Vol. 12, No. 5 (2016), pp. 580-588
DOI: 10.1007/s13391-016-6036-y

Microstructure and Micromorphology of Cu/Co Nanoparticles: Surface Texture Analysis

Ştefan Ţălu,[1] Miroslaw Bramowicz,[2] Slawomir Kulesza,[3] Atefeh Ghaderi,[4] Vali Dalouji,[5] Shahram Solaymani,[4,*] and Zahra Khalaj[6]

[1]Department of AET, Faculty of Mechanical Engineering, Technical University of Cluj-Napoca, Cluj-Napoca 400641, Romania
[2]Faculty of Technical Sciences, University of Warmia and Mazury in Olsztyn, Olsztyn 10-719, Poland
[3]Faculty of Mathematics and Computer Science, University of Warmia and Mazury in Olsztyn, Olsztyn 10-710, Poland
[4]Young Researchers and Elite Club, Kermanshah Branch, Islamic Azad University, Kermanshah 6718997551, Iran
[5]Department of Physics, Malayer University, Malayer 65719-95863, Iran
[6]Physics Department, Shahr-e-qods branch, Islamic Azad University, Tehran 13115-37541, Iran

(received date: 12 February 2016 / accepted date: 30 May 2016 / published date: 10 September 2016)

This paper analyses the three-dimensional (3-D) surface texture of Cu/Co thin films deposited by DC-Magnetron sputtering method on the silicon substrates. The prepared Cu/Co nanoparticles were used as research materials. Three groups of samples were deposited on silicon substrates in the argon atmosphere and gradually cooled down to room temperature. The crystalline structures and elemental compositions were analyzed by X-ray diffraction (XRD) spectrum with conventional Bragg-Brentano geometry. X-ray diffraction profile indicates that Co and Cu interpenetrating crystalline structures are formed in these films. The sample surface images were recorded using atomic force microscopy (AFM) and analyzed by means of the fractal geometry. Statistical, fractal and functional surface properties of prepared samples were computed to describe major characteristics of the spatial surface texture of Cu/Co nanoparticles. Presented deposition method is a versatile, cost-effective, and simple method to synthesize nano- and microstructures of Cu/Co thin films. This type of 3-D morphology allows to understand the structure/property relationships and to investigate defect-related properties of Cu/Co nanoparticles. Presented results confirm the possibility of preparing high-quality Cu/Co nanoparticles via DC-Magnetron sputtering method on silicon substrates.

Keywords: Cu/Co nanoparticles, DC-magnetron sputtering, AFM, fractal analysis, 3-D surface micro morphology

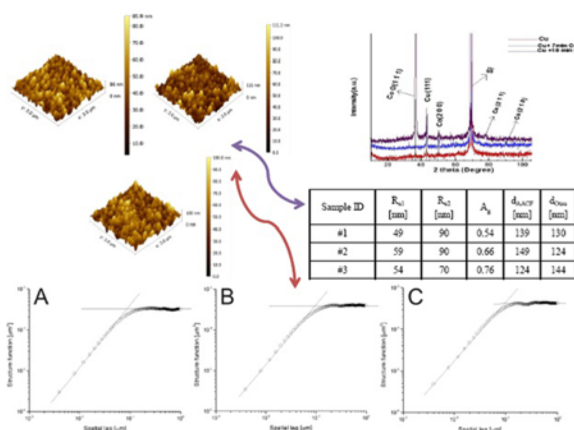

1. INTRODUCTION

Progress in the technology of thin films has drawn significant attention to various modifications of tailoring deposition techniques.[1-5] Considerable efforts have been directed toward understanding of key aspects of nonlinear dynamics of this phenomenon seen in electrical properties of interconnected micro- and nanostructures, complex geometry of metallic nanostructures etc.[6-9] The three dimensional (3-

*Corresponding author: shahram22s2000@yahoo.com
©KIM and Springer

D) surface morphology exerts significant influence on fundamental properties, and hence applicability, of thin films that combine electrical and magnetic properties, as well as the study and understanding of the mutual interactions between light, electricity, and magnetism at the nanometer scale.[10-14]

On the other hand, ongoing investigations and the description of processes occurring between and close to interacting surfaces that includes detachment and re-attachment of multiple microscopic contacts between surfaces of thin films in relative motion lead to concepts and new models based on the modern theories of multi-scale modelling.[15-20] The 3-D surface morphology of thin films is in correlation with the deposition method and can be classified as: isotropic (either Gaussian or non-Gaussian) or anisotropic.[21-23] It can be characterized using height images taken by atomic force microscopy (AFM)[24] in connection with fractal[1,4,7-9,16,22,23,25] and multifractal[3,5,10,12,13,15] geometry.

Even though surfaces of thin films are self-similar only in a restricted range of the spatial scales,[10,22,24] fractal geometry is useful for understanding the 3-D nanoscale architecture and phenomena concerning height variability. As such, fractal analysis might shed some light onto the dynamics of surface roughness change.[26]

In several past decades, numerous physical and chemical techniques have been proposed for the preparation of Cu/Co thin films.[27-31]

This work aims to analyze the Cu/Co nanoparticles deposited by DC-Magnetron sputtering method on the silicon substrates, to study their structure using XRD patterns, to discuss the LSPR peaks position by UV-visible spectra, and to characterize the 3-D surface texture using AFM data in connection with the statistical, and fractal analysis.

2. MATERIALS AND METHODS

2.1 Materials and preparation of thin films

Cu and Cu/Co nanoparticles were prepared using DC-Magnetron sputtering system on silicon substrates. Silicon was located on the grounded electrode, and Cu and Co targets (both 8 cm in radius) were attached to DC source (See Fig. 1). The chamber was evacuated to the pressure of 10.7×10^{-3} Pa before the deposition. Then, the chamber was filled with argon atmosphere that raised the pressure up to 2.6 Pa, and simultaneously the DC power was applied.

Film deposition was carried out at room temperature (297 ± 1 K) maintaining constant distance between electrodes. In the first stage that took 15 min with the voltage applied 500 V, substrate was covered with the material sputtered from Cu target. Then, the target was replaced with Co and the deposition process went on with the same voltage for another 7 and 10 min to reach Co/Cu bilayer thin film with varying Co thickness. Details of a sputtering process are given in Table 1.

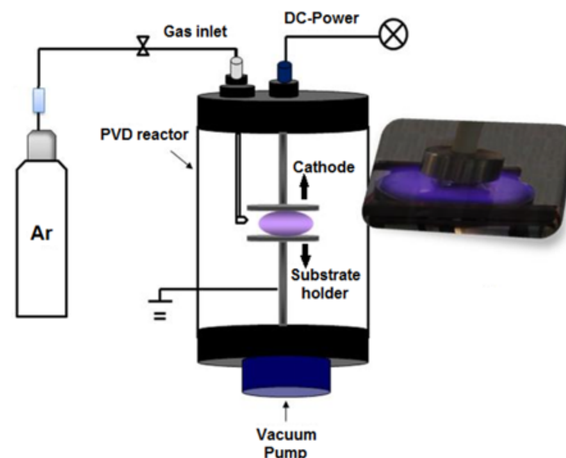

Fig. 1. Schematic diagram of the sputtering system.

Table 1. Sample IDs and details of a preparation procedure.

ID	Target	Sputtering parameters: Basic pressure [Pa]	Sputtering parameters: Work pressure [Pa]	Sputtering parameters: Power [W]	Deposition time [min]
#1	Cu	10.7×10^{-3}	2.6	16	15
#2	Cu/Co	10.7×10^{-3}	2.6	25	15/7
#3	Cu/Co	10.7×10^{-3}	2.6	25	15/10

2.2 Characterization of the thin film properties

Obtained samples were characterized by X-ray Diffraction (XRD) and Atomic Force Microscopy (AFM). X-ray diffraction data were recorded using CuKα radiation with the wavelength of 0.154 nm. AFM measurements were carried out in non-contact mode using Multimode instrument (Digital Instruments, Santa Barbara, CA) that scanned over 3 μm × 3 μm square areas of the sample surface with the rate 10-20 μm/s to obtain 256 × 256 pixel images.

The experiments were carried out at room temperature using cantilevers with the nominal properties for force-distance curve measurements specified in Ref. [32]. Then, The surface of Cu and Cu/Co thin films samples were scanned by Field Emission Scanning Electron Microscopy (FESEM, ZEISS SIGMA-VP).

2.3 Characterization of the film surface texture

AFM measurements sample surface topography resulting in data series of discrete height values. Prior to any analysis, however, it is necessary to get rid of the longest wavelength components that make the sampled surface non-stationary. Obtained series $z(x, y)$ is referred to as the residual surface, which in the following serves as a source of data for

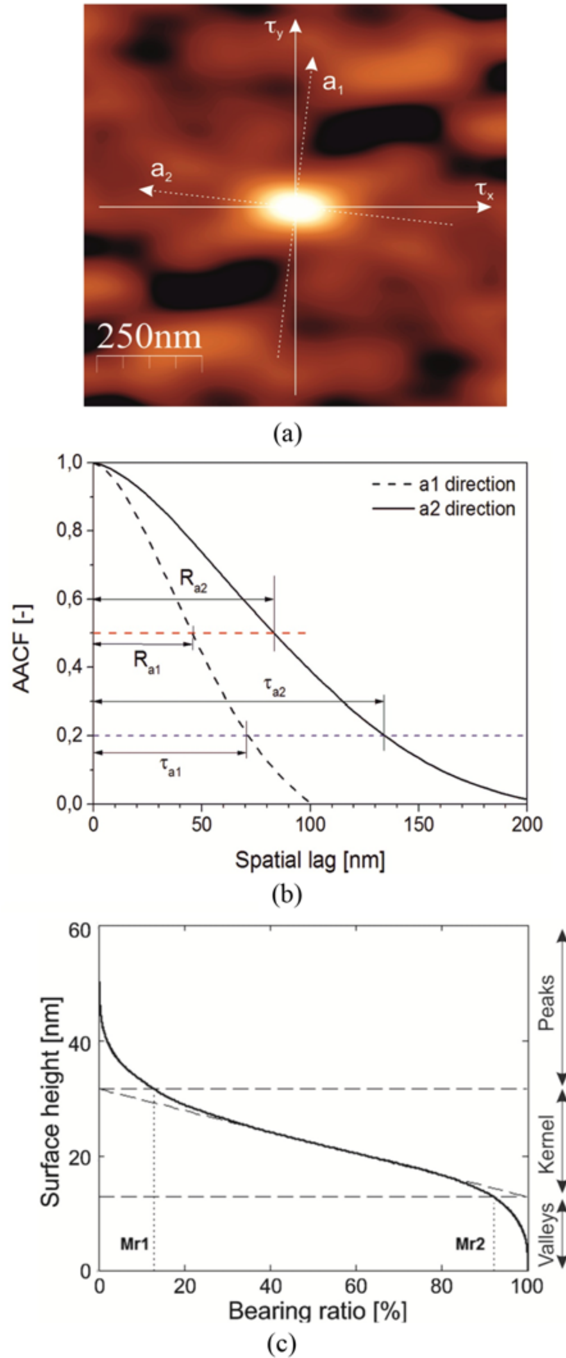

Fig. 2. (a) A map of AACF explaining directions of the fastest and slowest decays, respectively: a_1 and a_2; (b) Plots explaining decays lengths τ_{a1} and τ_{a2} along extreme decay directions and the estimation of grain radii R_{a1} and R_{a2}; (c) The plot of the Firestone-Abbott curve explaining main functional characteristics of the surface.

calculating normalized Areal Autocorrelation Function (AACF) $R(\tau_x, \tau_y)$[33] (Fig. 2a):

$$R(\tau_x, \tau_y) = \frac{\langle (z(x,y) - \langle z \rangle) \cdot (z(x+\tau_x, y+\tau_y) - \langle z \rangle) \rangle}{S_q^2} \quad (1)$$

Which in : $\langle \ldots \rangle$ - shows the mean value, the root-mean-square surface (RMS) roughness (normalizing term) is shown by S_q, whereas (τ_x, τ_y) – vector of a discrete spatial shift (space lag). S_q roughness is a standard deviation of surface height samples defined as:

$$S_q = \sqrt{\langle (z(x,y) - \langle z \rangle)^2 \rangle} \quad (2)$$

A map of AACF is then used to compute the surface texture ratio S_{tr} defined as the ratio of extreme auto-correlation decay lengths τ along which the normalized AACF falls from 1.0 down to 0.2 (see Fig. 2b):

$$0 < S_{tr} = \left.\frac{\tau_{a1}}{\tau_{a2}}\right|_{R=1\to 0.2} \leq 1 \quad (3)$$

In the above formula, the axes of the fastest and the slowest AACF decays are specified by $a1$ and $a2$, respectively.[34] $S_{tr} > 0.5$ claims that the surface is isotropic, while $S_{tr} < 0.3$ strongly shows an anisotropic surface.

To determine the grain dimension the plot of the AACF is used. Finally, the half-widths of the AACF profiles at half maxima along extreme directions are the grain radii R_{a1} and R_{a2}, respectively, this sum gives the average grain diameter (Fig. 2b):

$$d_{AACF} = R_{a1} + R_{a2} \quad (4)$$

Because of the stationary state of the residual surface so, the Structure Function (SF) is computed using:[35]

$$S(\tau_x, \tau_y) = 2S_q^2(1 - R(\tau_x, \tau_y)) \quad (5)$$

By plotting radially-averaged profile of a structure function on a log-log scale, fractal dimension D and corner frequency τ_c can be derived, because SF obeys the scaling law in the form:[35]

$$S(\tau) = K\tau^{2(2-D)} \quad (6)$$

where D – is the fractal dimension, and K – pseudo-topothesy. In the limit of a long wavelength (large spatial lags τ), however, this behavior breaks down, and the structure function asymptotically approaches $2S_q^2$ value. A point, at which this transition occurs is referred to as the corner frequency τ_c.

Functional parameters can be derived from the Firestone-Abbott also known as the bearing curve (see Fig. 2c) all explanations in this regard can be found in our previous publications.[36,37]

2.4 The Minkowski functionals

In this study, a set of the Minkowski Functionals (MFs)[3,38] that includes volume V, surface S and Euler-Poincaré

characteristic (or connectivity number χ), are computed and plotted using the Gwyddion 2.28 software.[39] This set can be expressed as:[39]

$$V = N_{white}/N;\ S = N_{bound}/N;\ \chi = (C_{white} - C_{black})/N \quad (7)$$

where: N - the total number of pixels; N_{white} - the number of 'white' pixels, that is pixels above the threshold (pixels below the threshold are referred to as 'black'); N_{bound} - the number of white-black pixel boundaries; C_{white} and C_{black} - the number of continuous sets of white and black pixels respectively.

2.5 Statistical analysis

Statistical analyses were performed using the GraphPad InStat version 3.20 computer software package (GraphPad, San Diego, CA, USA). Analysis of variance (ANOVA), followed by a post-hoc Tukey's test, was used to determine if there was a difference in the average parameters values between the different examined surface regions.

The differences in the average parameters values for a particular surface region were also analyzed using ANOVA and Tukey's test. A P value of less than 0.05 denoted the presence of a statistically significant difference.

3. RESULTS

The X-ray diffraction measurements shown in Fig. 3 were performed to study the microstructure of prepared samples of Cu/Co nanoparticles deposited by DC-Magnetron sputtering method on the silicon substrates, as it is summarized in Table 2. The peak at 67 ° is associated with silicon substrate.

Figure 4 presents representative 3 μm × 3 μm AFM images of the residual surfaces of Cu/Co nanoparticles

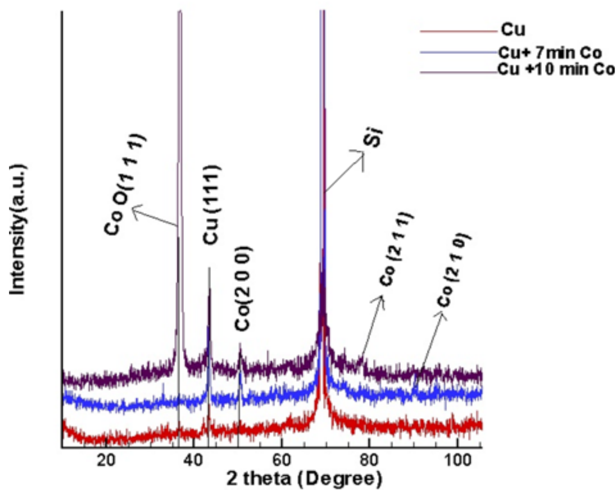

Fig. 3. XRD patterns of samples of Cu/Co nanoparticles on silicon substrate.

Table 2. Details of XRD pattern.

Sample	2θ peak position (degree)	(hkl)
#1	43	(111) Cu
#2	50	(200) Co
	90	(210) Co
#3	36	(111) CoO
	50	(200) Co
	78	(211) Co

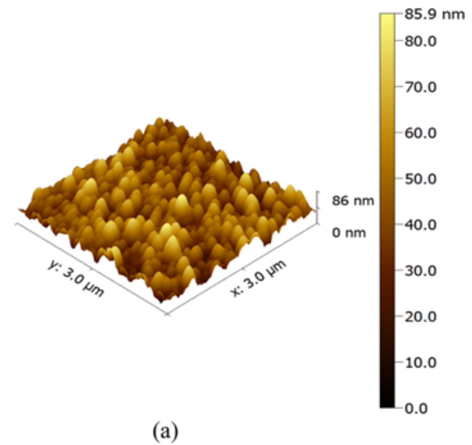

(a)

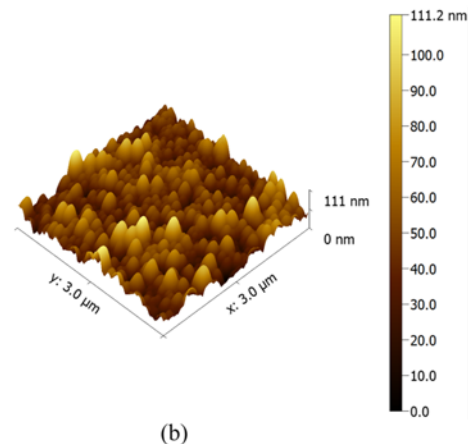

(b)

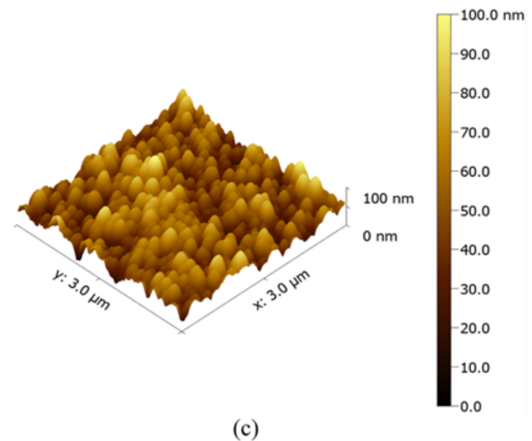

(c)

Fig. 4. 3 × 3 μm^2 AFM images of residual surfaces of Cu/Co nanoparticles: (a) sample #1, (b) sample #2, (c) sample #3.

Table 3. Estimated grain sizes.

Sample ID	R_{a1} [nm]	R_{a2} [nm]	A_g	d_{AACF} [nm]	d_{Otsu} [nm]
#1	49	90	0.54	139	130
#2	59	90	0.66	149	124
#3	54	70	0.76	124	144

R_{a1}, R_{a2} – grain radii equal to half-widths of the AACF profiles along extreme decay directions, A_g – asymmetry factor, d_{AACF} – average grain size from the AACF, d_{Otsu} – equivalent grain size estimated using Otsu's algorithm

Table 4. Statistical and fractal parameters of Cu/Co samples.

Sample ID	Sq [nm]	Kurt	Skew	S_{tr}	D	K [nm]	τ_c [nm]
#1	12.1	0.00	0.32	0.53	2.31	14	84
#2	15.0	1.06	0.75	0.68	2.31	16	95
#3	14.0	-0.06	0.17	0.79	2.33	13	95

S_q – RMS roughness, Kurt – kurtosis, Skew – skewness, S_{tr} – surface anisotropy ratio, D – fractal dimension, K – pseudo-topothesy, τ_c – corner frequency.

deposited by DC-Magnetron sputtering method on silicon substrates.

Table 3 summarizes grain sizes determined from the FWHM of the autocorrelation function and using Otsu's method. In turn, Table 4 summarizes main statistical and fractal characteristics of investigated samples.

Radially-averaged plots of the structure function of Cu/Co nanoparticles are shown in Fig. 5.

Table 5 summarizes main functional parameters derived from the Firestone-Abbott curve.

Figures 6-8 show the MFs, functions $V(z)$, $S(z)$, and $c(z)$,

Table 5. Functional parameters.

Sample ID	S_k [nm]	S_{pk} [nm]	S_{vk} [nm]	M_{r1} [%]	M_{r2} [%]
#1	34.10	20.10	19.29	11.06	92.41
#2	32.22	31.12	32.35	13.61	92.08
#3	39.21	18.49	40.00	11.06	92.80

S_k – kernel roughness depth, S_{pk} – reduced peak height, S_{vk} – reduced valley depth, M_{r1}/M_{r2} – upper/lower bearing area.

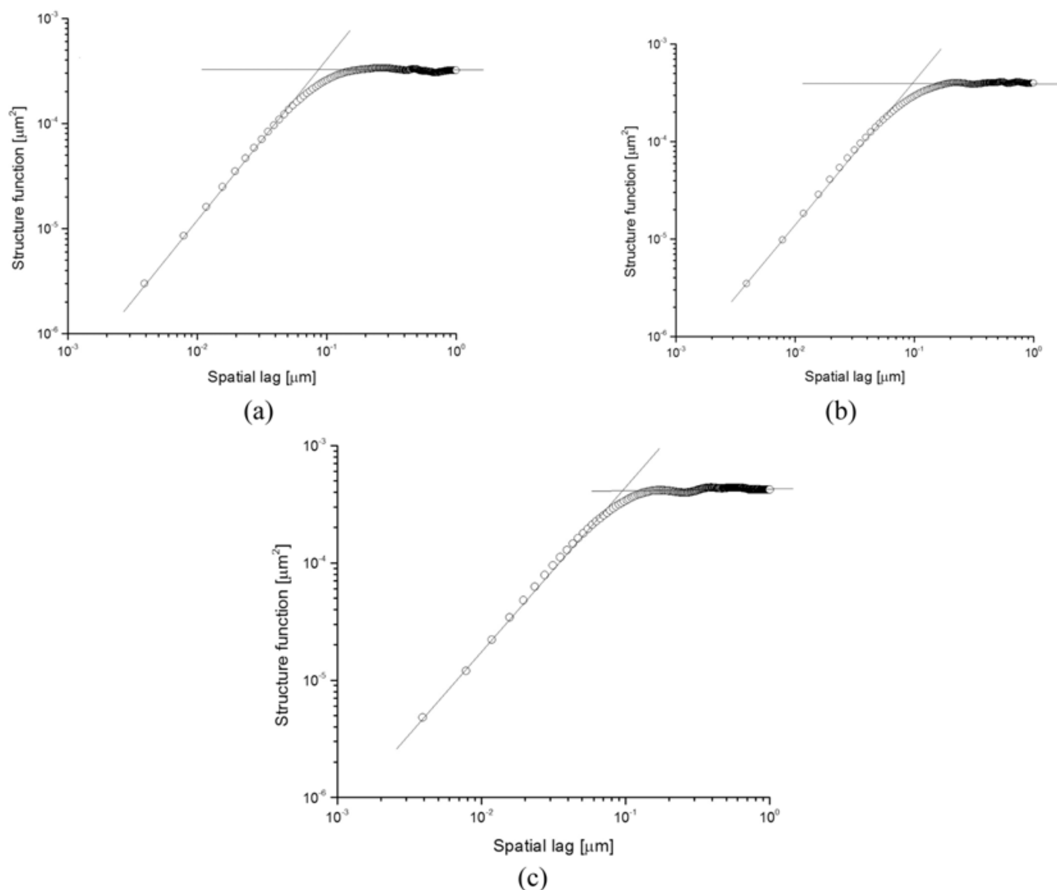

Fig. 5. Radially-averaged plots of the structure function of Cu/Co nanoparticles: (a) sample #1, (b) sample #2, (c) sample #3. Inclined parts of the plot are specific of fractal behavior described by fractal dimension D and pseudo-topothesy K, whereas flat ones saturate at $2S_q^2$ value. Transition point between these two regimes establishes corner frequency τ_c.

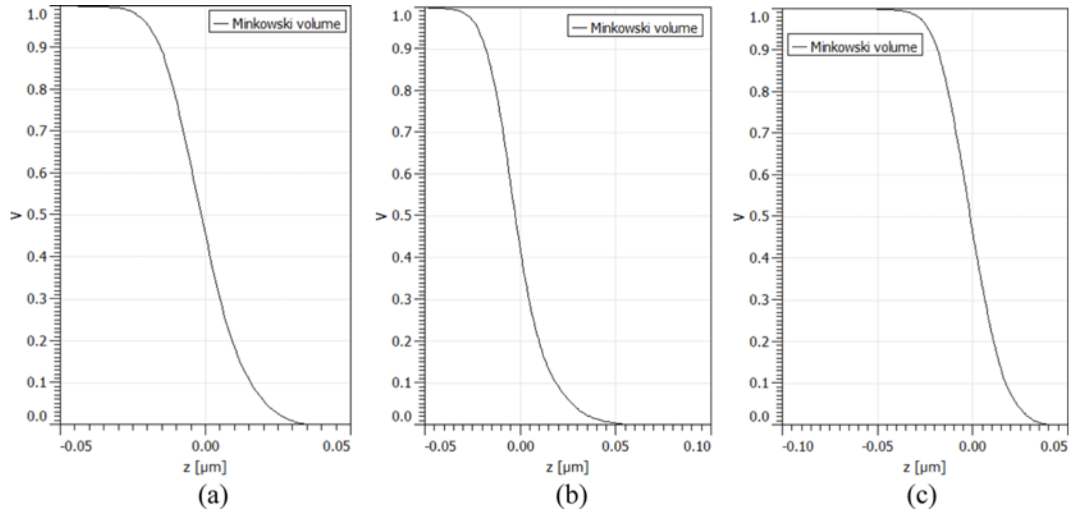

Fig. 6. Unitless Minkowski volume *V*(*z*) for the scanning areas of 3 μm × 3 μm of the sample: (a) #1, (b) #2, and (c) #3.

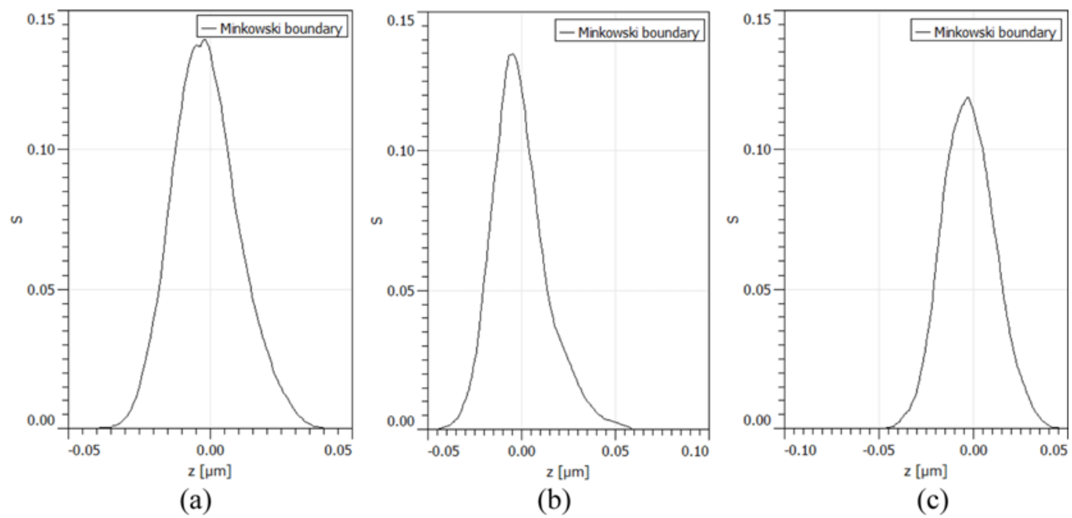

Fig. 7. Unitless Minkowski surface *S*(*z*) for the scanning areas of 3 μm × 3 μm of the sample: (a) #1, (b) #2, and (c) #3.

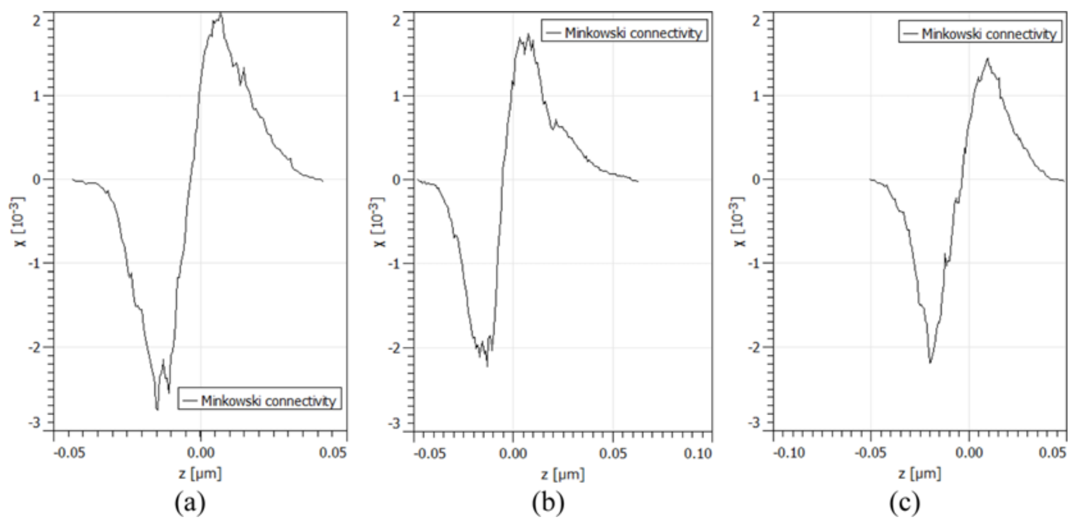

Fig. 8. Unitless Minkowski connectivity *c*(*z*) for the scanning areas of 3 μm × 3 μm of the sample: (a) #1, (b) #2, and (c) #3.

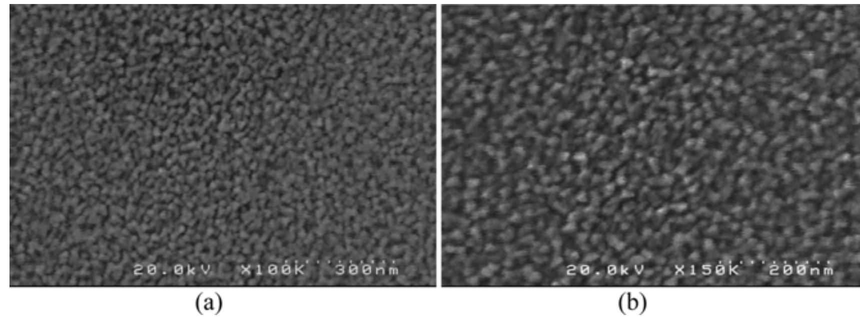

Fig. 9. Typical FESEM micrographs of samples (a) #1 and (b) #2.

plotted for the scanning areas of 3 μm × 3 μm: a) #1, b) #2, c) and #3, (associated with Fig. 4). These functions are unitless.

The typical FESEM images of Cu and Cu/Co nanoparticles, samples #1 and #2 are shown in Fig. 9(a) and (b), respectively. The shown images of both samples are in good agreement with presented AFM images.

4. DISCUSSION

AFM images in Fig. 4 exhibit granular surface structure of the samples under study composed of a large number of circular, 150 nm wide particles covering the entire substrate. High-order alignment can be also seen in Fig. 4, because the particles form linear chains with 3-4 beads. All the particles have the same orientation giving rise to strong crystalline texture. Interestingly, neither the particle size nor their shape change with elapsed time, which might be astonishing considering the results of XRD measurements and expectation that the grain size should generally increase during the growth process.

However, grain size presented in Table 3 and estimated using two independent methods agree well with the main topographical features seen in the AFM images. Regardless of the method, grain dimensions fall in the range from 120 to 150 nm and remain constant during the process. The difference is, however, that the AACF method gives insight into the grain elongation, i.e. their ellipsoidal shape, whereas the Otsu's method treats grains as perfect circles.

The former method allows us to conclude on the geometrical anisotropy of the particles (A_g parameter), which is found to increase from 0.54 (moderately anisotropic particles) to 0.76 (isotropic particles) and is equal to the anisotropy ratio of the entire surface (S_{tr} parameter shown in Table 4).

RMS surface roughness S_q turns out to be around 14 nm and constant among the samples (Table 4). On the other hand, measured height samples appear to follow Gaussian distribution in terms of kurtosis (except for sample #2), with a longer tail extending towards higher numbers (positive skewness). Particles turn from elliptical into more circular ones during the sputtering process since the surface anisotropy ratio steadily increases from 0.53 to 0.79. As mentioned previously, S_{tr} remains nearly identical to grain dimension anisotropy A_g, which is not surprising since both parameters were derived using different parts of the same AACF profiles.

On the other hand, fractal analysis reveal monofractal structure of the samples under study according to specific, monoclinic shape of the structure function drawn on a log-log plot in Fig. 5. Fractal dimension D that describes the scaling exponent of the surface remains constant at about 2.31. The same behavior concerns pre-scaling term, pseudo-topothesy K, which stays unchanged at around 14 nm. Corner frequency also varies only slightly at around 90 nm, which is about 60-70 per cent of the estimated grain dimension.

Similar proportion between these two parameters was demonstrated in our previous studies of Fe nanoparticles[1] that suggest it might be of universal character relating topographical features with their autocorrelation characteristics.

According to results from Table 5, kernel roughness depth S_k remains constant at around 35 nm, that is one-third of measured surface variation. Reduced peak height S_{pk} achieves significantly less values, around 20 nm except for the sample #2. On the other hand, reduced valley depth S_{vk} doubles during the sputtering process increasing from 20 nm for sample #1 to 40 nm for sample #3. Remaining parameters, upper and lower bearing areas, do not vary among samples, and are equal to, respectively, 11 per cent and 92 per cent similar to our previous study of Fe nanoparticles.[1]

Topological characteristics proved to be significant for characterization of the 3-D local topography of the sample surfaces.[40] The functions $V(z)$, $S(z)$, and $c(z)$ allowed a reasonable good prediction of the 3-D pattern at a nanoscale resolution corresponding to the size of the structural units which are relevant.

It can be seen that for a scanning area of 3 μm × 3 μm, the Minkowski volume $V(z)$ curve decreases slowly (from 1.0 to 0.95), then it decreases rapidly to zero for the z profile range:

a) from −0.015 to 0.035; b) from −0.015 to 0.055; c) from −0.015 to 0.040; and then it remains constant (Fig. 6). $V(z) > 0$.

It can be seen that for a scanning area of 3 μm × 3 μm, the Minkowski surface $S(z)$ curve rapidly increases to a maximum value of: a) 0.145 (for $z = -0.005$ μm); b) 0.135 (for $z = -0.01$ μm); c) 0.17 (for $z = -0.01$ μm); then rapidly decreases and tends to zero for $z = 0.05$ μm (Fig. 7). $S(z) > 0$.

The Minkowski connectivity describes the connectivity of spatial patterns that is particularly sensitive to topological changes of the pattern. Different types of micro-domains have different values of the local Euler-Poincaré characteristic. This demonstrates that such a measure can well discriminate between different morphologies (Fig. 8).

It can be seen that for a scanning area of 3 μm × 3 μm, the Minkowski connectivity $c(z)$ curve has an oscillation form with a minimum value of:

a) −2.7 (for $z = -0.015$ μm) and a maximum value of 2.0 (for $z = 0.09$ μm) (Fig. 8, a).

b) −2.3 (for $z = -0.015$ μm) and a maximum value of 1.8 (for $z = 0.09$ μm) (Fig. 8, b).

c) −2.2 (for $z = -0.020$ μm) and a maximum value of 1.5 (for $z = 0.09$ μm) (Fig. 8, c).

The values for $c(z)$ are positive for the ranges:

a) $-0.01 \le z \le 0.04$ (Fig. 8, a); b) $-0.01 \le z \le 0.06$ (Fig. 8, b); $-0.01 \le z \le 0.04$ (Fig. 8, c);

A negative value of connectivity number χ indicates a predominance of valleys, the minimum χ represents the maximum density of valleys and the maximum value of χ is equal to the maximum density of peaks. The maximum densities of peaks and valleys values should be taken into account in technical applications.

Modeling and quantifying spatial heterogeneity is useful to systematically investigate the relation of topology and effective surface properties.

5. CONCLUSIONS

The objective of this study was to study the three-dimensional (3-D) surface texture of Cu/Co nanoparticles deposited by DC-Magnetron sputtering method on the silicon substrates. The characterizations were carried out using X-ray diffractometer, AFM, and fractal analyses.

Our results also suggest that AFM, statistical, fractal and functional surface properties of Cu/Co nanoparticles deposited by DC-Magnetron sputtering method on silicon substrates can be useful to obtain structural information from local sampling and to a better understanding of the effects, spatial scaling, and correct interpretation of surface topographic features as well as its functional role for the test surface.

These results can be applied in thermodynamic and kinetic models of electronic, atomic and vibrational structure of Cu/Co nanoparticles, as well as in study of surface energy, surface tension, surface stress, surface diffusion, and structural forces to elucidate the stability of Cu/Co nanoparticles. Also, the 3-D surface texture of nanostructures estimated by specific parameters can be included in accurate and robust mathematical models to describe bridging the gap between the nano, micro and macro scales in friction, new approaches to control and modify frictional properties involved at nanometer-scale resolution of thin films.

Declaration of interest: The authors report no conflict of interests. The authors alone are responsible for the content and writing of the paper.

REFERENCES

1. Ş. Ţălu, M. Bramowicz, S. Kulesza, A. Shafiekhani, A. Ghaderi, F. Mashayekhi, and S. Solaymani, *Ind. Eng. Chem. Res.* **54**, 8212 (2015).
2. S. Stach, Ż. Garczyk, Ş. Ţălu, S. Solaymani, A. Ghaderi, R. Moradian, Negin B. Nezafat, S. M. Elahi, and H. Gholamali, *J. Phys. Chem. C* **119**, 17887 (2015).
3. V. Dalouji, S. M. Elahi, S. Solaymani, and A. Ghaderi, *Eur. Phys. J. Plus.* **131**, 84 (2016).
4. S. Kim, K. Hyun, J. Y. Moon, C. Clasen, and K. H. Ahn, *Langmuir* **31**, 1892 (2015).
5. S. Stach, S. Roskosz, J. Cybo, and J. Cwajna, *Mater. Charact.* **60**, 1151 (2009).
6. K. Srinivas, M. Manivel Raja, D. V. Sridhara Rao, and S. V. Kamat, *Thin Solid Films* **558**, 349 (2014).
7. Y. Chen, F. Yang, Y. Dai, Y. Wang, and S. Chen, *J. Phys. Chem. C* **112**, 1645 (2008).
8. A. Pankiew, W. Bunjongpru, N. Somwang, S. Porntheeraphat, S. Sopitpan, J. Nukaew, C. Hruanun, and A. Poya, *J. Microscopy Society of Thailand* **24**, 103 (2010).
9. J. H. Byeon and J. W. Kim, *ACS Appl. Mater. Inter.* **2**, 947 (2010).
10. G. Amarandei, C. O'Dwyer, A. Arshak, and D. Corcoran, *ACS Appl. Mater. Inter*. **5**, 8655 (2013).
11. S. Solaymani, A. Ghaderi, and N. B. Nezafat, *J. Fusion Energ.* **31**, 591 (2012).
12. N. Ghobadi, M. Ganji, C. Luna, A. Arman, and A. Ahmadpourian, *J. Mater. Sci. Mater. El.* **27**, 2800 (2016).
13. Ş. Ţălu, S. Stach, A. Mahajan, D. Pathak, T. Wagner, A. Kumar, R. K. Bedi, and M. Ţălu, *Electron. Mater. Lett.* **10**, 719 (2014).
14. Y. Reyes-Vidal, R. Suarez-Rojas, C. Ruiz, J. Torres, Ş. Ţălu, A. Méndez, and G. Trejo, *Appl. Surf. Sci.* **342**, 34 (2015).
15. Ş. Ţălu, S. Stach, A. Méndez, G. Trejo, and M. Ţălu, *J. Electrochem. Soc.* **161**, D44 (2014).
16. M. Pelliccione and T.-M. Lu, *Evolution of Thin Film Morphology: Modeling and Simulation,* 1st ed., pp. 11-12, Springer-Verlag New York, New York, USA (2008).

17. D. Elenkova, J. Zaharieva, M. Getsova, I. Manolov, M. Milanova, S. Stach, and Ş. Ţălu, *Int. J. Polym. Anal. Ch.* **20**, 42 (2015).
18. M. Molamohammadi, A. Arman, A. Achour, B. Astinchap, A. Ahmadpourian, A. Boochani, S. Naderi, and A. Ahmadpourian, *J. Mater. Sci. Mater. El.* **26**, 5964 (2015).
19. S. Ramazanov, Ş. Ţălu, D. Sobola, S. Stach, and G. Ramazanov, *Superlattice. Microst*. **86**, 395 (2015).
20. S. Naderi, A. Ghaderi, S. Solaymani, and M. M. Golzan, *Eur. Phys. J. Appl. Phys.* **58**, 20401 (2012).
21. Ş. Ţălu, *Micro and Nanoscale Characterization of Three Dimensional Surfaces. Basics and Applications,* Napoca Star Publishing House, Cluj-Napoca, Romania (2015).
22. M. Bramowilcz, S. Kulesza, T. Lipiński, P. Szabracki, and P. Piątkowski, *Sol. St. Phen.* **203-204**, 86 (2013).
23. S. Kulesza and M. Bramowicz, *Appl. Surf. Sci.* **293**, 196 (2014).
24. M. Bramowicz, S. Kulesza, and K. Rychlik, *Techn. Sc*. **15**, 307 (2012).
25. K. Wasa, M. Kitabatake, and H. Adachi, *Thin Film Materials Technology: Sputtering of Control Compound Materials*. Co-published by: William Andrew, Inc. Norwich, NY, USA and Springer-Verlag GmbH & Co., Heidelberg, Germany (2004).
26. R. P. Yadav, M. Kumar, A. K. Mittal, and A. C. Pandey, *Chaos* **25**, 083115 (2015).
27. T. Elko-Hansen, A. Dolocan, and J. G. Ekerd, *J. Phys. Chem. Lett.* **5**, 1091 (2014).
28. R. G. Gordon, H. Kim, and H. Bhandari, *US Patent* 8461684 (2013).
29. A. Kohn, M. Eizenberg, and Y. Shacham-Diamand, *J. Appl. Phys.* **94**, 3015 (2003).
30. A. Kohn, M. Eizenberg, Y. Shacham-Diamand, and Y. Sverdlov, *Mat. Sci. Eng. A* **302**, 18 (2001).
31. S. B. Lim, A. Rahtu, and R. G. Gordon, *Nat. Mater*. **2**, 749 (2003).
32. B. Bhushan, H. Fuchs, and S. Kawata, *Applied Scanning Probe Methods V*, Springer: Heidelberg, Germany (2007).
33. P. R. Nayak, *J. Lubrication Tech.* **93**, 398 (1971).
34. W. P. Dong, P. J. Sullivan, and K. J. Stout, *Wear* **178**, 45 (1994).
35. A. Thomas and T. R. Thomas, *J. Wave Material Interaction* **3**, 341 (1988).
36. Ş. Ţălu, S. Solaymani, M. Bramowicz, N. Naseri, S. Kulesza, and A. Ghaderi, *RSC Adv.* **6**, 27228 (2016).
37. Ş. Ţălu, M. Bramowicz, S. Kulesza, S. Solaymani, A. Shafikhani, A. Ghaderi, and M. Ahmadirad, *J. Ind. Eng. Chem.* **35**, 158 (2016).
38. R. J. Adler and J. E. Taylor, *Random Fields and Geometry,* Springer, New York, USA (2007).
39. P. Klapetek, D. Nečas, and C. Anderson, *Gwyddion Software User Guide,* version 2.28, http://gwyddion.net/ (2012).
40. H.-J. Vogel, *Topological Characterization of Porous Media*, pp. 75-92, Springer-Berlin Heidelberg, Germany (2002).